ELSEVIER

Materials Science and Engineering A 429 (2006) 79–89

MATERIALS SCIENCE & ENGINEERING A

www.elsevier.com/locate/msea

Elastic limit at macroscopic deformation of icosahedral Al–Pd–Mn single quasicrystals

L. Ledig, M. Bartsch, U. Messerschmidt *

Max-Planck-Institut für Mikrostrukturphysik, Weinberg 2, D-06120 Halle/Saale, Germany

Received 1 April 2006; accepted 22 May 2006

Abstract

$Al_{70.5}Pd_{21}Mn_{8.5}$ single quasicrystals were plastically deformed between 482 and 821 °C. The strain rate sensitivity of the flow stress was measured by stress relaxation tests. At several temperatures, the dislocation structures were imaged by diffraction contrast in a high-voltage electron microscope for determining the dislocation densities. At all temperatures, the plastic deformation starts with a range of very high work-hardening. The transition point between almost elastic and elastic–plastic deformation is called the elastic limit. At low temperatures, the deformation was stopped at about 1.5 GPa to prevent fracture. Above about 580 °C, the stress–strain curves bend down and show a yield point effect followed by a range of almost steady state deformation. At low temperatures, the elastic limit is much lower than the steady state flow stress or the maximum stresses reached without fracture. The activation parameters are different for the elastic limit, the range of high work-hardening and steady state deformation. The flow stresses are interpreted by the stress necessary to move individual dislocations and the athermal component due to the elastic interaction between dislocations. At low temperatures, a further component is necessary to explain the very high flow stresses reached by work-hardening.

Keywords: Quasicrystals; Plastic deformation; Dislocations; Transmission electron microscopy

1. Introduction

From earlier studies it is well established that, at a fixed strain rate, icosahedral Al–Pd–Mn single quasicrystals show different plastic behaviour depending on the temperature. In most cases, however, the plastic deformation starts with a range of very high work-hardening. At low temperatures, this results in high stresses at quite low plastic strains until the specimens break at a stress in the order of magnitude of about 1.6 GPa [1]. At high temperatures, dynamic recovery leads to lower stresses so that the deformation curve goes through a maximum, the upper yield point, and ends up in a range of almost steady state deformation, where the work-hardening is balanced by the recovery. Most deformation studies on Al–Pd–Mn single quasicrystals are concerned with this type of deformation [2–5]. Sometimes, even a range of work-softening follows (e.g. [6,7]). The transition point between almost elastic loading and the range of strong work-hardening was observed before [4] but not studied in detail. In this paper, new deformation experiments were carried out to establish the temperature dependence of this transition point and to compare it with other flow stress data.

The mode of dislocation motion in icosahedral quasicrystals is not fully clear, yet. The dislocations move on well-defined crystallographic planes [8] so that glide was considered the dominating mode. Only very recently, experiments proved dislocations moving by pure climb in icosahedral Al–Pd–Mn [9,10] though other experiments show also the contribution of glide [11,12]. If climb is fast enough, other structural features may control the dislocation mobility, the cluster structure [13–15] or a Peierls mechanism either on the atomic [16] or the cluster scale [17]. All these mechanisms are thermally activated so that the flow stress can be described by the formalism below.

The total flow stress σ of quasicrystals is supposed to be represented by

$$\sigma = \sigma^* + \sigma_\mathrm{i} + \sigma_\mathrm{ph} \tag{1}$$

where σ^* is the effective stress necessary to move the dislocations at the imposed velocity. It results from an Arrhenius-type relation of the thermally activated dislocation motion:

$$\sigma^* = \frac{1}{V_\mathrm{ex}} \left(\Delta F + kT \ln \frac{\dot{\varepsilon}}{\dot{\varepsilon}_0} \right) \tag{2}$$

* Corresponding author. Tel.: +49 345 558250; fax: +49 345 5511223.
E-mail address: um@mpi-halle.de (U. Messerschmidt).

0921-5093/$ – see front matter © 2006 Elsevier B.V. All rights reserved.
doi:10.1016/j.msea.2006.05.126

Here, ΔF is the Helmholtz free energy of activation, k the Boltzmann factor, T the absolute temperature, $\dot{\varepsilon}$ the plastic strain rate, and $\dot{\varepsilon}_0$ is the so-called pre-exponential factor, containing the mobile dislocation density. V_{ex} is the experimental activation volume, which can be determined from the strain rate sensitivity of the flow stress $r = \Delta\sigma/\Delta \ln \dot{\varepsilon}$ by

$$V_{ex} = kT\frac{\Delta \ln \dot{\varepsilon}}{\Delta\sigma} = \frac{kT}{r} \tag{3}$$

The second contribution in Eq. (1) is the athermal stress component σ_i arising from the long-range elastic interaction between dislocations. It is also called the internal stress and can be estimated from the dislocation density ρ by the Taylor formula for a random arrangement of parallel dislocations [18]:

$$\sigma_i = \frac{\alpha\mu b\rho^{1/2}}{m} \tag{4}$$

α is a numerical constant between 0.2 and 1, μ the shear modulus, and b is the parallel component of the Burgers vector. A similar equation is obtained for the interaction between intersecting dislocations of different Burgers vectors. The formula is originally derived for glide, where m is the orientation factor of the respective slip system. However, the equation can also be applied to climb or a combination of climb and glide on defined planes. The geometrical factor may assume similar values for this case. The stress component τ_{ph} may originate from the work necessary to form phason faults in the wake of the moving dislocations.

In addition to the macroscopic mechanical data, dislocation densities were measured from high-voltage transmission electron micrographs of samples deformed at different temperatures to estimate the athermal part of the flow stress according to Eq. (4). On the basis of these experiments, it is tried to interpret the plastic processes at the early stages of deformation and to assess the different contributions to the flow stress of Al–Pd–Mn single quasicrystals.

2. Experimental

Icosahedral single quasicrystals of the composition $Al_{70.5}Pd_{21}Mn_{8.5}$ were obtained from the Jülich quasicrystals research group. They were grown by the Czochralski or Bridgman methods. For the compression tests, rectangular specimens were cut by a wire saw. The face normals were chosen parallel to highly symmetrical directions of the quasicrystal structure with compression axes in two-fold or five-fold directions. No differences were observed between the deformation data of these two orientations. After carefully grinding and polishing the faces, the specimens had dimensions of 4.5–8 mm in length and 1.5–4.5 mm^2 for the cross-section. Particular attention was paid on the grip faces to be exactly plane and parallel to avoid deviations from the elastic range at the beginning of deformation. The samples were deformed in a digitally controlled single-screw testing machine. The closed-loop control of the machine was based on the position l of the hot anvils measured by a magnetic differential transducer. This kind of control results in a large effective stiffness. If l_0 is the starting length of the sample, the total (engineering) strain is given by

$$\varepsilon_t = \frac{\Delta l}{l_0} \tag{5}$$

The experiments were performed at total strain rates between $\dot{\varepsilon}_t = 10^{-4}\,s^{-1}$ and $10^{-6}\,s^{-1}$ in the temperature range from 821 down to 482 °C, the lowest temperature where plastic deformation without destroying the samples was still possible. The (engineering) flow stress σ for plastic deformation depends on the strain rate and the temperature and was calculated from the measured force F on the specimen and the cross-section area A_0 of the undeformed sample as

$$\sigma = \frac{F}{A_0} \tag{6}$$

During deformation at these high temperatures in air, a thin oxide layer formed on the sample surfaces. Therefore, some specimens were deformed in an argon atmosphere. However, there are no differences in the results for deformation in air or argon. Thus, these two deformation conditions will not be distinguished further. The present paper includes also earlier deformation data from the studies described in [1,4,5].

To measure the strain rate sensitivity of the flow stress $r = d\sigma/d\ln \dot{\varepsilon}$, stress relaxation tests were performed at different stages of the deformation. The relaxation rate was plotted versus the stress. In these plots, the strain rate sensitivity is given by the reciprocal value of the slope of the curves, $r = d\sigma/d\ln(-\dot{\sigma})$.

For transmission electron microscopy, the samples were cooled down inside the deformation machine before unloading, so that the dislocation microstructure is frozen-in. The deformed samples were cut by a wire saw into slices about 0.3 mm thick with their normal parallel either to the deformation axis or perpendicular to it in high-symmetry directions. After grinding, dimpling and electrolytical jet polishing, the dislocation microstructure was imaged in diffraction contrast in a high-voltage electron microscope (HVEM) at an acceleration voltage of 1000 keV. The high acceleration voltage allows to investigate relatively thick sample areas, where the dislocation structure should correspond to that of bulk samples.

3. Results

3.1. Macroscopic deformation data

Typical stress–strain curves of the material are shown in Fig. 1, where the flow stress σ is plotted versus the total strain ε_t. Fig. 1a presents an example of 487 °C, which is almost the lowest temperature achieved in this study. Since the specimens are very brittle at these low temperatures, low total strain rates were applied, mostly $\dot{\varepsilon}_t = 10^{-6}\,s^{-1}$. There appears a knee in the deformation curve, which marks a transition from almost elastic to elastic–plastic deformation with a very high rate of work-hardening. This transition is called here the elastic limit and labelled EL in Fig. 1. It corresponds to an instantaneous increase in the plastic strain rate. As shown in Fig. 1a, the elastic limit is determined as the intersection between tangents to the

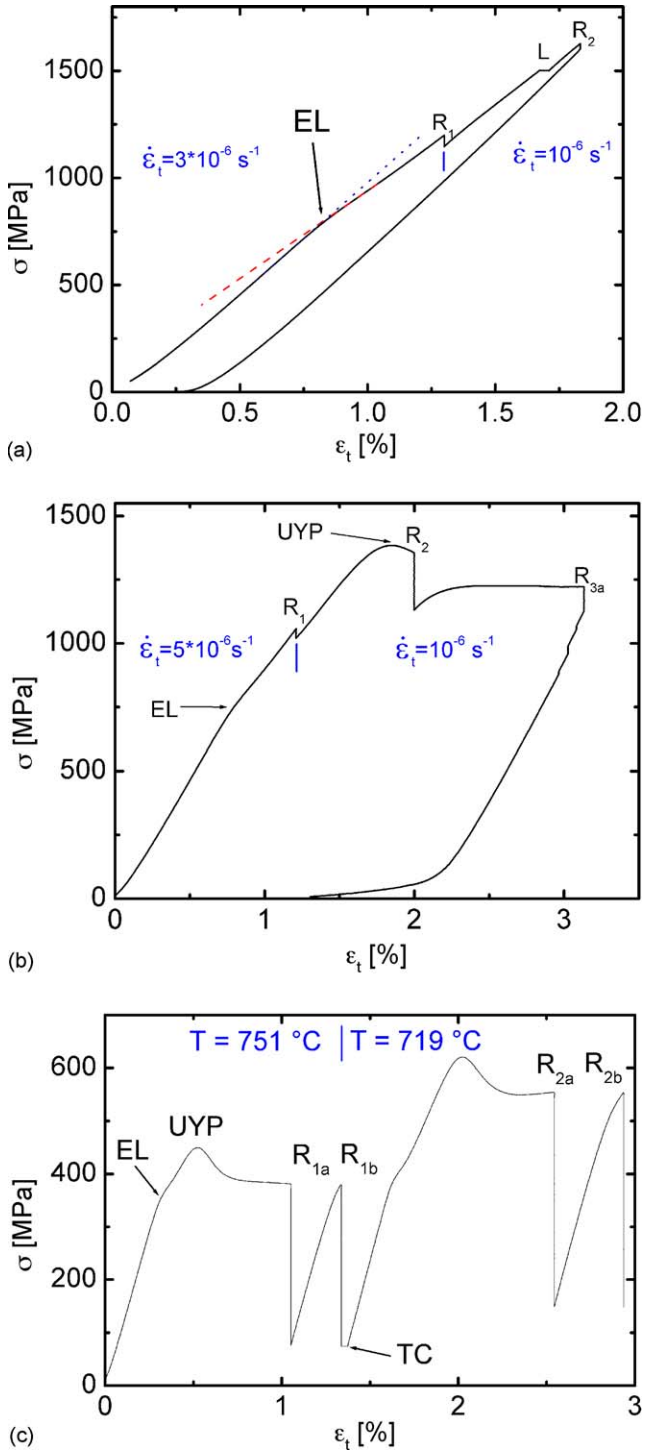

Fig. 1. Stress–strain curves at different temperatures including stress relaxation tests R_x. (a) $T = 487\,^{\circ}\mathrm{C}$, $\dot{\varepsilon}_t = 3 \times 10^{-6}\,\mathrm{s}^{-1}$ and change to $10^{-6}\,\mathrm{s}^{-1}$ as well as some deformation under constant load (L). (b) $T = 580\,^{\circ}\mathrm{C}$, $\dot{\varepsilon}_t = 5 \times 10^{-6}\,\mathrm{s}^{-1}$ and change to $\dot{\varepsilon}_t = 10^{-6}\,\mathrm{s}^{-1}$. (c) $T = 751\,^{\circ}\mathrm{C}$ and change to $T = 719\,^{\circ}\mathrm{C}$, $\dot{\varepsilon}_t = 10^{-4}\,\mathrm{s}^{-1}$.

stress–strain curve before (dotted line) and after the transition point (dashed line). Below 550 °C, the experiments were stopped at stresses around 1.5 GPa to prevent fracture. For measuring the strain rate sensitivity of the flow stress, stress relaxation tests R_x were carried out by keeping the total strain ε_t constant. These tests increase the plastic strain at low strain rates. Additional plastic deformation can also be obtained under creep conditions at constant range (L).

Fig. 1b shows the stress–strain curve for deformation at 580 °C. At increasing strain, the curve bends down, goes through a maximum, the upper yield point (UYP), and ends up in a range of almost steady state deformation. During steady state deformation, the work-hardening is balanced by recovery. The temperature of Fig. 1b is the lowest one where the upper yield point was overcome before sample failure. The stress at the elastic limit is much lower than the steady state flow stress. During the stress relaxation R_2 performed after the upper yield point, the stress relaxes much more than during the relaxation R_1 in the initial work-hardening range. Both relaxations were stopped at about $\ln(\dot{\sigma}\,[\mathrm{MPa\,s^{-1}}]) = -3$, corresponding to a plastic strain rate of about $5 \times 10^{-7}\,\mathrm{s}^{-1}$.

Going to higher temperatures, the steady state flow stress decreases drastically, so that it becomes only slightly higher than the elastic limit, as demonstrated in Fig. 1c for 751 °C at a strain rate of $\dot{\varepsilon}_t = 10^{-4}\,\mathrm{s}^{-1}$. In this experiment, a temperature change experiment TC was performed to the lower temperature of 719 °C. This is connected with an increase in the flow stress. During the second deformation into the steady state, a yield drop effect occurs again. Apart from these changes of the deformation conditions, the flow stress reaches a steady state value after passing the yield drop, which is characteristic of the deformation at high temperatures. Such deformation curves are described in most papers on quasicrystal deformation. A distinct initial range of high work-hardening appears not in all experiments. It is pronounced in specimens with a two-fold compression axis.

Fig. 2 shows a summary of the temperature dependence of the elastic limit and of the steady state flow stress. Both decrease at increasing temperature. As mentioned above, the steady state flow stress is only slightly greater than the stress at the elastic limit for temperatures above about 650 °C and a strain rate

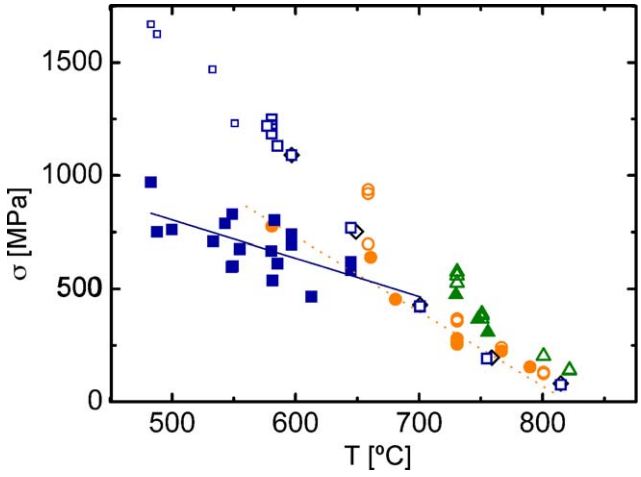

Fig. 2. Temperature dependence of the steady state flow stress (open symbols) and the elastic limit (full symbols). The four small open symbols at low temperatures correspond to the maximum stresses reached in the experiments where steady state flow was not achieved. The total strain rates $\dot{\varepsilon}_t$ are $10^{-6}\,\mathrm{s}^{-1}$ (squares, dark blue), $2 \times 10^{-6}\,\mathrm{s}^{-1}$ (diamonds, black), $10^{-5}\,\mathrm{s}^{-1}$ (circles, orange) and $10^{-4}\,\mathrm{s}^{-1}$ (triangles, olive). The straight lines represent linear regression curves through the elastic limits measured at $10^{-5}\,\mathrm{s}^{-1}$ (full line, dark blue) and $10^{-6}\,\mathrm{s}^{-1}$ (broken line, orange).

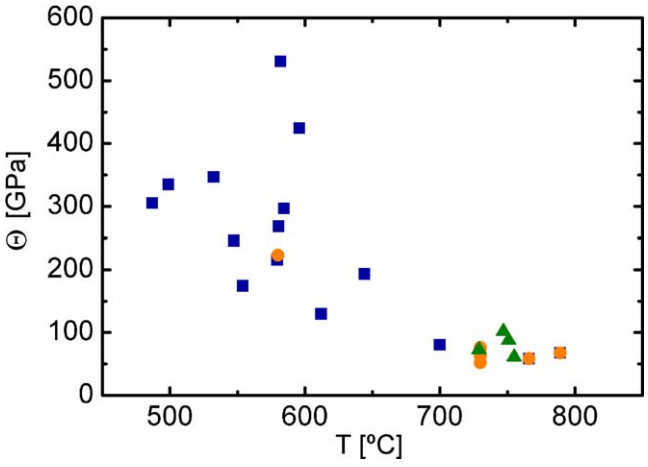

Fig. 3. Temperature dependence of the work-hardening coefficient $\Theta = d\sigma/d\varepsilon$. ε is the plastic strain.

of $10^{-5}\,s^{-1}$. For lower temperatures, however, the difference between both increases with decreasing temperature. At a total strain rate of $10^{-6}\,s^{-1}$, the elastic limit becomes equal to the steady state flow stress at 700 °C and is not observed above this temperature. The small open symbols below 570 °C, where steady state deformation was not achieved because of the brittleness of the specimens, correspond to the maximum stresses reached in these deformation tests still before the upper yield point.

As mentioned above and plotted in Fig. 3, the work-hardening coefficient $\Theta = d\sigma/d\varepsilon$ decreases with increasing temperature. ε is the plastic strain. Θ is in the range of the elastic modulus S of the specimen and the parts of the deformation machine inside the strain measurement circuit. S is measured from the slope of the unloading curves at the end of the experiments. The stiffness values increase with decreasing temperature between about 80 and 120 GPa. Thus, $\Theta \cong S$ at high temperatures and $\Theta \cong 3S$ at low ones.

As described in Section 2 and shown in Fig. 1, stress relaxation tests were performed during all experiments to study the strain rate sensitivity r of the flow stress. Fig. 4a presents three relaxation curves measured above the elastic limit within the work-hardening range at the low temperature of 547 °C. These curves are almost straight and shifted along the stress axis corresponding to the work-hardening during deformation. Fig. 4b shows respective curves taken from an experiment in the high-temperature range (760 °C). The first relaxation R_1 is performed below the elastic limit. It is steep like the curves at low temperatures but demonstrates that at high temperatures the specimens deform plastically with a low rate even in the "elastic" range. At low temperatures, practically no relaxation occurs at much higher stresses. Above the elastic limit, in the work-hardening range, the relaxation curve R_2 starts still with a steep range but afterwards bends to a second range of low slope. This transition is due to recovery becoming important at low relaxation rates. The curve R_6 is the first one measured in the range of steady state deformation. The steep initial range has almost disappeared. Further curves exhibit only the flat part. Strain rate sensitivity data were always measured from the slope at the

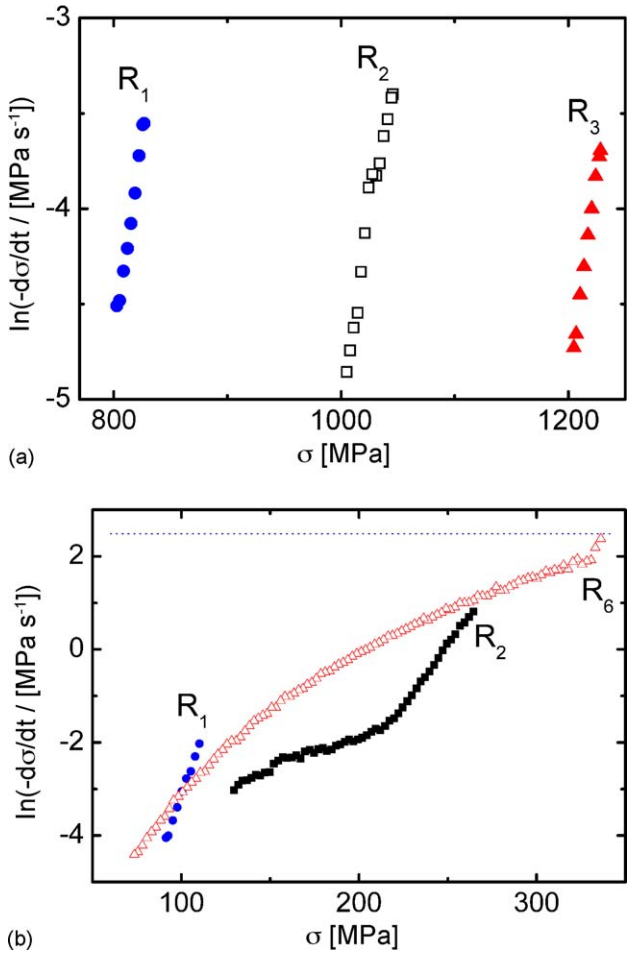

Fig. 4. Stress relaxation curves taken at different stages of deformation and at different temperatures. (a) $T = 547$ °C. Relaxations taken above the elastic limit at different plastic strains. The total strain rate $\dot{\varepsilon}_t$ before the relaxations corresponds to $\ln(-\dot{\sigma}) = -2.23$. (b) $T = 760$ °C. R_1: relaxation taken below the elastic limit; R_2: above the elastic limit within the work-hardening range; R_6: first relaxation in the steady state range of deformation. The horizontal dotted line corresponds to the total strain rate $\dot{\varepsilon}_t$ before the relaxations.

beginning of the curves. Thus, they correspond to the strain rate before the relaxations. Because of the very high values of the work-hardening coefficient in the work-hardening range of the deformation curves (Fig. 3), the work-hardening during the relaxation tests leads to a pronounced decrease of the relaxation rate. Therefore, the strain rate sensitivity data have to be corrected according to

$$r = r_{ex}\left(\frac{1+\Theta}{S}\right) \tag{7}$$

With the values of Θ and S quoted above, this correction is essential. All strain rate sensitivity data are collected in Fig. 5. The data from steady state deformation (open symbols) increase with decreasing temperature and increasing total strain rate. Those obtained from the work-hardening range (full symbols) show the same tendency but are lower than the steady state ones.

In order to estimate the activation energy of the elastic limit (EL), its temperature sensitivity $\Delta\sigma_{EL}/\Delta T$ was determined by linear regression analysis of the data in Fig. 2. It

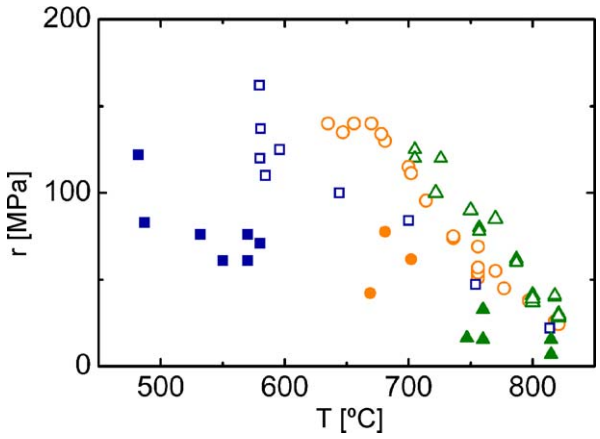

Fig. 5. Strain rate sensitivity of the flow stress vs. temperature: (full symbols) stress relaxation tests during the (initial) work-hardening range, the experimental data are corrected for work-hardening; (open symbols) relaxation tests during steady state deformation; (squares) $\dot{\varepsilon}_t = 10^{-6}\,s^{-1}$; (circles) $\dot{\varepsilon}_t = 10^{-5}\,s^{-1}$; (triangles) $\dot{\varepsilon}_t = 10^{-4}\,s^{-1}$. The values for steady state deformation at 10^{-4} and $10^{-5}\,s^{-1}$ are from Ref. [4].

amounts to $-3.3\,MPa\,K^{-1}$ for the high-temperature range and $\dot{\varepsilon}_t = 10^{-5}\,s^{-1}$ and to $-1.69\,MPa\,K^{-1}$ for the low temperature range at $\dot{\varepsilon}_t = 10^{-6}\,s^{-1}$. The regression straight lines are included in Fig. 2. The data are listed in Table 1. In a few experiments, the temperature sensitivity was measured at low temperatures by temperature change tests in the work-hardening range (TC whr). Since the plastic strain rate may change during a temperature change test, the stress difference $\Delta\sigma$ due to the temperature change was taken from stress relaxation curves just before and after the temperature change at the same relaxation rate. Between the two relaxations, the specimens harden so that $\Delta\sigma$ has to be corrected for the work-hardening by an amount of $\Theta\,\Delta\varepsilon$. The necessary work-hardening coefficients were determined from the stress difference for the same relaxation rate in two relaxation curves taken at the same temperature. The average of the temperature sensitivity of three tests is included in Table 1. Two temperature change experiments were carried out in the steady state range (TC ss) at low temperatures. $\Delta\sigma$ was taken again between relaxation curves. However, no corrections were made because of the steady state deformation. The results are also listed in Table 1.

3.2. Dislocation microstructure and density

In order to characterize the dislocation microstructures and to estimate the athermal stress component σ_i by means of Eq. (4), dislocation structures were studied in the HVEM. Fig. 6a shows the dislocation structure formed at 482 °C, the lowest deformation temperature achieved. The image plane is a cross-sectional plane with its normal parallel to the five-fold compression axis. Strongly bowed dislocations enclose areas of relatively uniform contrasts. Stereo pairs show that the enclosed areas are roughly plane but that the individual bulges frequently point out of this plane. Of two sets of dislocations, the directions of the parallel components of the Burgers vectors were determined by contrast extinctions. Both parallel components were of two-fold directions which enclosed an angle of 58° with the five-fold compression axis. Fig. 6b presents the dislocation structure of the experiment with the deformation curve in Fig. 1b performed at the lowest temperature were steady state deformation was reached, i.e. at 580 °C. The dislocation structure consists of deformation bands with a high density of dislocations. The planes on which the dislocations extend are steeply inclined. It is obvious that many dislocations exhibit curved segments at this temperature. The dislocation density was determined inside the bands. Weak contrasts originate partly from contrast extinction but inside the bands mostly from the excitation of weak reflections. Fig. 6c shows an example from steady state deformation in the high-temperature range. In this case, the dislocation structure consists of a homogeneous network of dislocations of different Burgers vectors as observed before [12,19]. Many dislocations are straight and oriented crystallographically. Part of the dislocations is imaged by very weak contrast because of contrast extinction. The dislocation densities were determined by counting the number of intersections of the dislocation lines with a net of straight lines of arbitrary orientation. The dislocation density is then given by [20]:

$$\rho = f\frac{2N_S}{L_S t} \tag{8}$$

N_S is the number of dislocation intersections with lines of the length L_S. The sample thickness t was estimated from micrographs with dislocation structures of a known geometry to be about 0.5 μm. f is a correction factor of 1.84 introduced in [21] to consider the number of extinguished dislocations. The dislocation density is plotted in Fig. 7 versus the temperature. Open symbols mark measurements after deformation in the steady state range at $\dot{\varepsilon}_t = 10^{-5}\,s^{-1}$, which strongly increase with decreasing temperature. The full symbols represent data from low temperatures in the range of high work-hardening. These values are low because of the small plastic strains of 0.07–0.35% reached in these samples without steady state defor-

Table 1
Activation energies and related data

Experiment type	T (°C)	$\dot{\varepsilon}_t$ (s^{-1})	$\Delta\sigma/\Delta T$ ($MPa\,K^{-1}$)	r (MPa)	ΔH (eV)	σ (MPa)	ΔW (eV)
EL	690	10^{-5}	−3.3	63	3.88	425	0.56
EL	560	10^{-6}	−1.69	70	1.44	689	0.70
TC whr	564	10^{-6}	−3.54	70	3.05	918	0.95
TC ss	664	10^{-5}	−12.4	153	6.13	888	0.47
TC ↑ ss	580	2×10^{-6}	−10	107	5.86	1170	0.80

EL: elastic limit, $\Delta\sigma/\Delta T$ from linear regression of elastic limit data; TC whr: temperature change during the work-hardening range, average of three temperature changes; TC ss: change to higher temperature during the steady state range, single experiment.

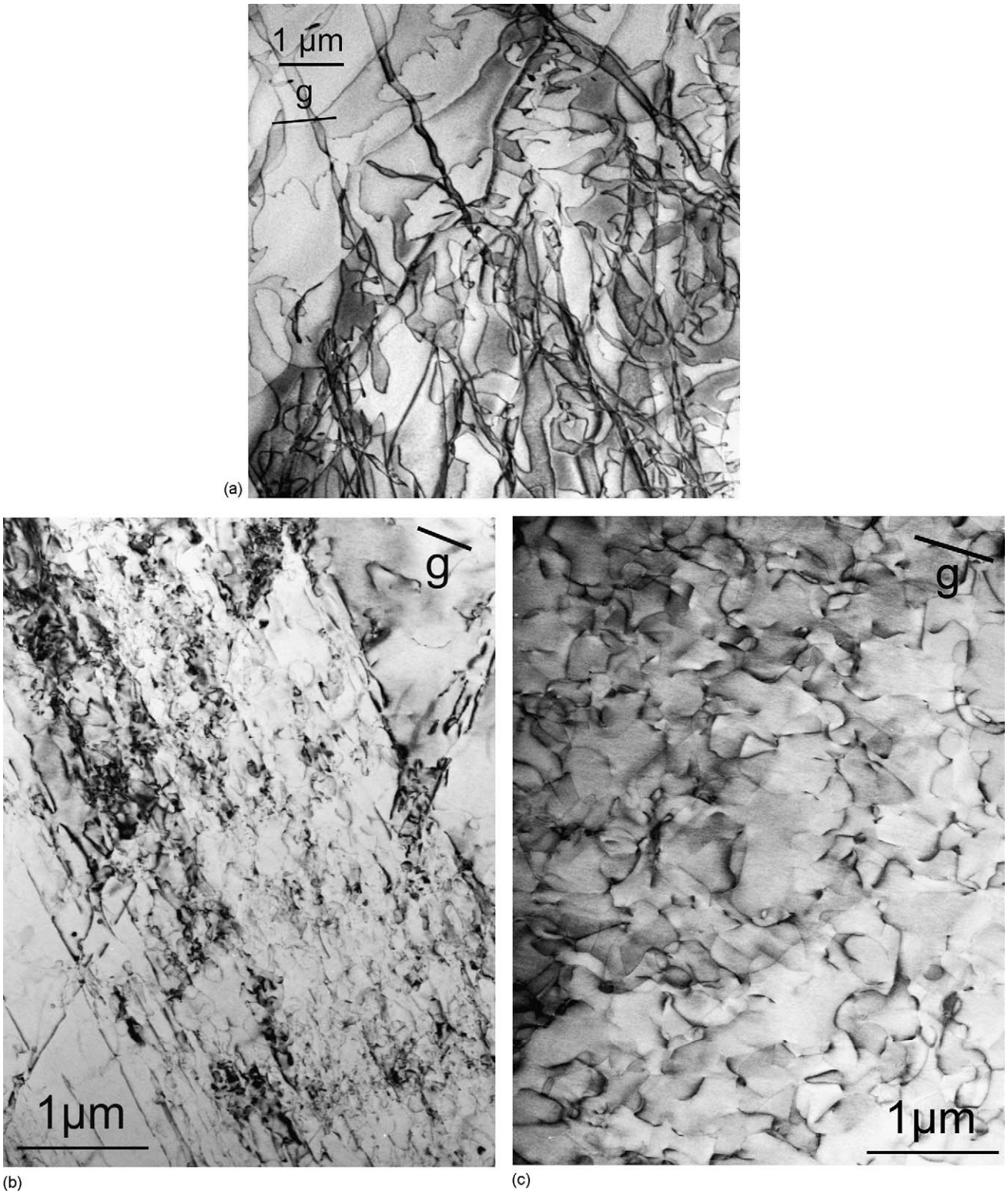

Fig. 6. Bright field HVEM micrographs of deformed samples. (a) $T = 482\,^{\circ}\mathrm{C}$, $\dot{\varepsilon}_t = 10^{-6}\,\mathrm{s}^{-1}$, plastic strain $\varepsilon = 0.35\%$. Two-fold **g** vector near the five-fold pole corresponding to the foil normal and the deformation axis. (b) Sample of Fig. 1b, $T = 580\,^{\circ}\mathrm{C}$, $\dot{\varepsilon}_t = 10^{-6}\,\mathrm{s}^{-1}$, $\varepsilon = 2\%$. Five-fold **g** vector near the two-fold pole corresponding to the foil normal and the deformation axis. (c) $T = 730\,^{\circ}\mathrm{C}$, $\dot{\varepsilon}_t = 10^{-4}\,\mathrm{s}^{-1}$, $\varepsilon = 6\%$. Two-fold **g** vector near the two-fold pole corresponding to the foil normal and the deformation axis.

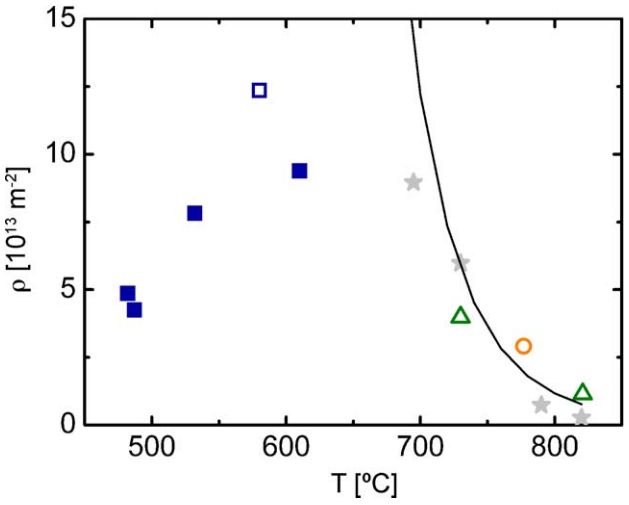

Fig. 7. Dislocation density vs. temperature for deformation in the steady state range (open symbols) and in the range of high work-hardening (solid symbols). Total strain rates as in Fig. 2. Gray asterisks show data from [23] for comparison. Black line: theoretical curve after the modelling in [20] for deformation at high temperatures.

mation. For comparison, Fig. 7 includes also steady state data of specimens quenched from the high deformation temperatures [22]. The present high-temperature data roughly agree with these data.

4. Discussion

4.1. Plastic strain rate

The observed elastic limits (Fig. 1) mark the transition from almost elastic deformation to plastic deformation with a very high work-hardening coefficient. While during steady state deformation (at high temperatures), the plastic strain rate $\dot{\varepsilon}$ equals the total strain rate $\dot{\varepsilon}_t$ imposed by the machine, this relation does not hold for the deformation with a high work-hardening rate as after the elastic limit. Generally, the plastic strain rate can be calculated using the slope of the deformation curve $d\sigma/d\varepsilon_t$ according to

$$\dot{\varepsilon} = \dot{\varepsilon}_t \left(1 - \frac{1}{S}\frac{d\sigma}{d\varepsilon_t}\right) = \dot{\varepsilon}_t \frac{S}{S+\Theta} \tag{9}$$

With the S values quoted above and Θ from Fig. 3, the plastic strain rate amounts to only about 50% of the total strain rate at high temperatures and to only 30% at the lowest one. However, since Θ is constant in the work-hardening range, $\dot{\varepsilon}$ is also constant. These reduced strain rates become evident from Fig. 4, where the relaxation curves start at much lower relaxation rates than those corresponding to the total strain rate. They have to be attributed to the mechanisms at the elastic limit, too.

4.2. The activation parameters

In the work-hardening range at low temperatures, the stress relaxation curves in Fig. 4a consist only of the steep part. This part defines the strain rate sensitivity r and accordingly the activation volume V_{ex} of the processes controlling the dislocation mobility. At high temperatures, the curve R_2 in Fig. 4b starts again with the steep part but exhibits also a flat part like the curves measured during steady state deformation (R_6). In the present representation, stress relaxation curves describing a single obstacle mechanism of the dislocation mobility should bend towards the stress axis approaching the athermal stress component, i.e. the strain rate sensitivity should decrease with decreasing load. However, the curves R_2 and R_6 show the opposite behaviour. This kind of relaxation curves is called recovery-type relaxations as pointed out in [23]. Accordingly, the flat part of the relaxation curves in Al–Pd–Mn quasicrystals is interpreted in [4,5] by dynamic recovery, in accordance with other experimental observations. Thus, at high temperatures recovery takes place already in the initial range of strong work-hardening. This is certainly the reason for the strong decrease of the work-hardening coefficient with increasing temperature (Fig. 3).

The activation volumes following from the strain rate sensitivity via Eq. (3) measured during steady state deformation are discussed in detail in [4,5,11,15,17]. Fig. 5 shows that the strain rate sensitivities obtained in the work-hardening range are essentially smaller than those in the steady state range. A quantity allowing some interpretation of the processes controlling the deformation is the so-called stress exponent $m' = d\ln\dot{\varepsilon}/d\ln\sigma = \sigma/r$. For $\dot{\varepsilon}_t = 10^{-6}\,s^{-1}$, the average value is $m' \cong 10$. This is larger than the values from steady state deformation at high temperatures of $m' \cong 5$ (e.g. [11]). As in both cases, the instantaneous strain rate sensitivity is assumed to be controlled by the dislocation mobility, there should be a change in the mechanism. Besides, m' is always far away from $m = 1$, which holds if climb controls directly the deformation rate. A more detailed analysis has to consider also the athermal stress contribution. However, as shown in Section 4.5, it is small and does not change the results drastically.

The activation enthalpy of deformation can be determined from the temperature dependence of the flow stress and the strain rate sensitivity according to

$$\Delta H = -\frac{kT^2}{r}\frac{\Delta\sigma}{\Delta T} \tag{10}$$

For the elastic limit, the temperature sensitivity $\Delta\sigma_{EL}/\Delta T$ was determined in Section 3.1 by regression of the data in Fig. 2. The related temperatures and stresses are taken at the centres of the regression lines. The values are listed in the first two lines of Table 1. No strain rate sensitivity data are available for the elastic limit. Thus, r values of the work-hardening range are taken as averages from the data in Fig. 5. They should be valid for the elastic limit, too, since r only weakly depends on the strain. The values of ΔH from the temperature change tests during the work-hardening and steady state ranges are also included in Table 1. In this case, the r values were measured from the stress relaxation tests before and after the temperature changes.

The part of the activation energy expended from the external stress is the so-called work term $\Delta W = V_{ex}\sigma^*$. With Eq. (3), it is

given by

$$\Delta W = \frac{kT\sigma^*}{r} \tag{11}$$

The data of ΔW are also listed in Table 1. For the elastic limit data, σ_{EL} is taken instead of σ^* and for the temperature change tests σ. Both approximations lead to an overestimation of ΔW. Nevertheless, the work term is only a small part of the activation energy.

Since in the high-temperature range the elastic limits are only slightly lower than the lower yield points, the present activation energy from the elastic limits taken at 690 °C and a nominal strain rate of $10^{-5}\,s^{-1}$ agrees well with the previous data from the steady state range [4,5] at the same temperature. Nevertheless, the physical meaning of the two quantities should be quite different. In the present case, the activation energy should describe the mobility of the dislocations while for the steady state range both the mobility of the dislocations and the recovery of the dislocation structure lead to some average between both activation energies [19]. The very low value of the activation energy for the low-temperature range measured at a nominal strain rate of $10^{-6}\,s^{-1}$ cannot easily be understood. This low value does not fit the still quite high temperatures. The change in the activation energy appears at about 650 °C and is accompanied with the change in the stress exponent. In the same range, recovery becomes unimportant at the usual strain rates ($\dot{\varepsilon} \geq 10^{-5}\,s^{-1}$) [4,5]. In addition, the change in the activation energy may also be connected with a change in the mechanisms controlling the dislocation mobility. Indeed, the shape of the dislocations is different in the two temperature ranges. At low temperatures, dislocations are frequently curved and trail planar faults (Fig. 6a and b) [12]. At high ones, planar faults are not observed and the dislocations are oriented along crystallographic directions, both when moving [8] as well as when they form a three-dimensional network as in Fig. 6b [20]. Speculations about the respective mechanisms are described in [11].

The activation energy from the temperature change tests in the work-hardening range is roughly equal to that of the elastic limit at high temperatures. However, the energies from the two new measurements in the steady state range at low temperatures are very high and do not fit the expectation of decreasing energies with decreasing temperature from the earlier measurements in [5] at higher temperatures. Nevertheless, they represent the strong temperature dependence of the steady state flow stresses in Fig. 2.

4.3. The athermal stress part due to elastic dislocation interactions

The athermal stress component σ_i due to the elastic interaction between dislocations is estimated from the dislocation densities plotted in Fig. 7 by using Eq. (4). Following the modelling of the steady state flow stresses in the high-temperature range in [19], the numerical factor α is set to unity. In this sense, the calculated values represent upper limits of σ_i.

The temperature dependence of the shear modulus was considered according to a power law regression of the data in [24] as

$$\mu(T) = 77.7452\,\text{GPa} - 0.014\,\text{GPa}\,\text{K}^{-1}T - 1.3 \times 10^{-5}\,\text{GPa}\,\text{K}^{-2}T^2 \tag{12}$$

T is measured in K. The absolute value of the Burgers vector is set to the frequently occurring value of $b = 0.183$ nm [25] and the geometrical factor to $m = 0.4$. This should be a good average for glide in the icosahedral structure with many slip systems of a high orientation factor and is sufficient for the rough estimate if climb is involved. Calculated values of σ_i are included in the diagram of Fig. 8 and are discussed in Section 4.5.

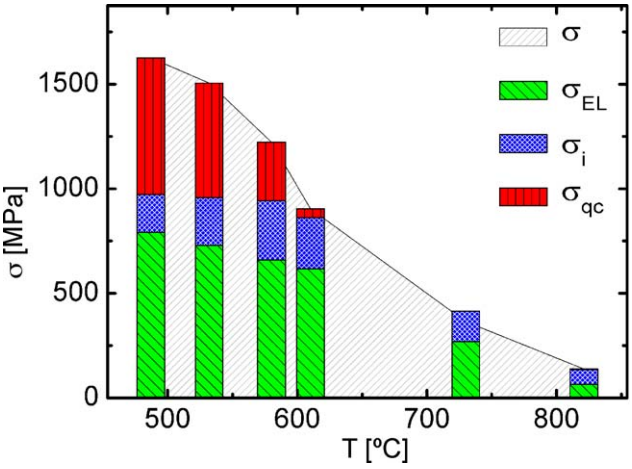

Fig. 8. Comparison of the different stress contributions over the whole temperature range of deformation. σ: total stress, σ_{EL}: elastic limit, σ_i: athermal stress, σ_{qc}: unknown stress component.

In the modelling mentioned above [19], the evolution of the dislocation density is described by a rate of formation of new dislocations by multiplication and a rate of dynamic recovery leading to a good representation of the experimental steady state flow stresses in the high-temperature range. The respective theoretical temperature dependence of the dislocation density is included in Fig. 7. It fits roughly the experimental high-temperature data. At low temperatures, however, the experimental values are much too low to explain the high stresses in this range, which develop in the course of the strong work-hardening.

4.4. The elastic limit

Below the elastic limit, the plastic strain rate is very low, especially at low temperatures where the specimens practically do not relax if the machine is stopped. At high temperatures, however, the specimens relax already below the elastic limit, as demonstrated in Fig. 4b. Nevertheless, the plastic strain rate increases above the elastic limit from a low value to the reduced rate discussed in Section 4.1. The stress σ_{EL} at the elastic limit has to be attributed to this strain rate. As shown in [22], dislocation multiplication starts from the low grown-in dislocation density only at proceeding plastic deformation. Thus, the athermal stress contribution due to elastic dislocation interactions is still small at the elastic limit. It may therefore be supposed that the latter corresponds to the intrinsic mechanisms determining

the dislocation motion at the velocity imposed by the plastic strain rate. After Eq. (1), this is the effective stress σ^* and the stress σ_{ph} necessary to produce phason defects in the wake of the moving dislocations:

$$\sigma_{EL} = \sigma^* + \sigma_{ph} \quad (13)$$

According to Eq. (2), σ^* represents a flow stress contribution depending on the temperature and the strain rate. While the main mode of dislocation motion in Al–Pd–Mn seems to be climb [9–12], the large stress exponent m' estimated in Section 4.2 and the crystallographic orientation of the dislocation lines during their motion on crystallographic planes [8] suggest that the dislocation mobility is controlled by other processes related to the quasicrystal structure. Possible mechanisms are discussed in [11,15]. This discussion is not a topic of the present paper.

The role of the phason contribution σ_{ph} is not clear. Starting with a dislocation in thermal equilibrium surrounded by a cloud of phason defects, at low temperatures the dislocation moving away carries only the phonon part of the Burgers vector if phason relaxations cannot occur fast enough. As a consequence, a layer of a high density of phason faults is created in the wake of the dislocation. The energies of the initial and final states of the dislocation are different resulting in a friction stress acting on the dislocation. This process is similar to the production of stacking faults and is therefore of energy storing character. Accordingly, it should not be of thermally activated nature. The necessary stress component is estimated in [15] to 135 MPa (with the geometric factor of $m = 0.4$). Thus, it would be an essential part of the total flow stress only at high temperatures. At low ones, the defects will accumulate in the lattice during deformation. As described in Section 4.5, the accumulating phason defects may cause the strong work-hardening at low temperatures.

Although the electron microscopy contrasts of the planar faults in Fig. 6a and b are not analyzed in detail, it is assumed that they represent the phason layers created by the moving dislocations. The present authors observed these defects only in the low-temperature range, i.e. at and below 610 °C but not in all deformed specimens [11,12,17]. At higher temperatures, the phason layers produced by moving dislocations disappear [26]. Observation of the data scattering in the speckle contrast of diffuse X-ray scattering shows that the phasons diffuse slightly more slowly than Mn atoms at about 650 °C [27]. Thus, phasons become mobile at roughly the same temperature where recovery by diffusion sets in. At high temperatures, the phason field belonging to the total Burgers vector diffuses with the dislocation. Thus, the energies of the dislocation in the initial state and in a state after some motion are equal (in an infinite body), yielding no flow stress contribution. The process may be compared with the high-temperature branch of the Cottrell effect, where the dislocation in equilibrium is surrounded by a cloud of foreign atoms (for a review see [28]). At high temperatures, the impurity cloud diffuses easily with the moving dislocation, also not causing a flow stress contribution. Going to lower temperatures, an incomplete cloud with the dislocation located out of the centre of the cloud impedes the dislocation motion. In quasicrystals, similarly the phason cloud around the dislocation is not in equilibrium and phason defects may be created individually and diffuse away. This process may be thermally activated and causes a flow stress contribution which, however, is always less than the athermal one at low temperatures. Nevertheless, such a contribution is considered in the modelling of high-temperature deformation of Al–Pd–Mn in [29,30]. A reduction of this component during straining by disturbing the ideal quasicrystal structure is considered to cause the work-softening observed in some experiments. However, in this paper it is argued that the phason part of the flow stress σ_{ph} can be neglected in the high-temperature range. The modelling of the temperature and strain rate dependence of the steady state flow stress mentioned in Section 4.2 [19] is possible without invoking a phason contribution [11,19].

4.5. The stress components

A summary of the different contributions to the flow stress is given in Fig. 8. The columns are plotted for temperatures where dislocation density data are available. At and below 610 °C, the data for the elastic limit σ_{EL} were taken from the regression straight line. The total flow stresses are the steady state values at high temperatures and the maximum stresses at and below 530 °C. A main part of the steady state flow stress at high temperatures is the elastic limit σ_{EL} which, according to the present interpretation, should essentially be controlled by the mobility of individual dislocations. Another contribution is the athermal component σ_i from elastic dislocation interactions calculated from the dislocation densities by Eq. (4). As discussed already before, no other component is necessary to interpret the deformation at high temperatures [19]. Below about 630 °C, the sum of these two stress components is clearly smaller than the flow stress, in the case of steady state flow down to 580 °C as well as at lower temperatures where steady state deformation could not be achieved. Thus, an additional flow stress component σ_{qc} has to be invoked which may be characteristic of quasicrystals at low temperatures. This stress component is not intrinsic to the motion of dislocations since it does not enter the elastic limit. Accordingly, it cannot be the phason component σ_{ph} introduced in Eq. (1). It develops only during deformation, i.e. by work-hardening. However, it is not due to usual elastic dislocation interactions since the observed dislocation densities are far too low to explain the very high flow stresses reached at low temperatures. There are two possibilities to explain the strong work-hardening at low temperatures.

The following interpretation is suggested here. At low temperatures, phason walls are created. This process causes an athermal stress contribution σ_{ph} which enters the elastic limit σ_{EL} but which is not essential. The main part of the elastic limit originates from the thermal friction stress σ^*. Because of the low mobility of the phasons, the phason walls accumulate during straining. The interaction between moving dislocations and the accumulating phason walls leads to a rapidly increasing stress component σ_{qc}. At present, a model of this interaction cannot be given. At the transition to the high-temperature range, both phasons and vacancies become mobile. Thus, the creation of phason defects does not cause a stress contribution and they do not accumulate any more. In addition, the diffusion of point

defects results in dynamic recovery. This interpretation of the role of phason damage stored in the quasicrystal structure is different from that suggested in [29,30] for the high-temperature range. Here, the phason damage stored during deformation is supposed to result in a reduction of σ_{ph} and accordingly to work-softening. However, in agreement with the present understanding and according to [26,27] phasons do not accumulate in the high-temperature range. Further studies are necessary to better understand these processes.

Another explanation may follow from the discussion in [31]. The climbing dislocations produce a sub- or supersaturation of vacancies, depending on the sign of the stress, compression or tension, respectively. At low temperatures where the mobility of vacancies is low so that the sub- or supersaturation does not recover, strong deviations from the thermal equilibrium concentration c_0 may be generated. This causes a chemical stress:

$$\sigma_c = \frac{kT}{\Omega} \ln \frac{c_0}{c} \tag{14}$$

where Ω is the atomic volume ($\cong 1.5 \times 10^{-29}\,m^3$) and c the actual vacancy concentration. With a stress component of $\sigma_{qc} \cong 500$ MPa at 530 °C (Fig. 8), the concentration ratio should be $c/c_0 \cong 0.5$. After a dilatometric study [32], the equilibrium concentration of thermal vacancies amounts to about $c_0 \cong 8 \times 10^{-5}$ at the same temperature. Thus, if the deformation occurs solely by climb and the deviations from the thermal defect equilibrium are stored, plastic strains of this order of magnitude are sufficient to induce such a high chemical stress. This model has certainly some problems. High diffusion coefficients are observed only for Al. Pd and Mn diffusion is about three orders of magnitude slower [33]. Besides, the deviations from the thermal equilibrium concentration should relax within a few hours at 530 °C [32] which the flow stress certainly does not.

5. Conclusions

- In the temperature range studied between 482 and 821 °C, plastic deformation of Al–Pd–Mn single quasicrystals, especially in the two-fold orientation, starts with a range of very high work-hardening. The stress at the transition between the elastic range and this work-hardening range is called the elastic limit.
- It is suggested that the elastic limit represents the stress necessary to move dislocations at the velocity imposed by the actual plastic strain rate. This involves an effective (thermally activated) stress to move the dislocations in the quasicrystal structure and a possible stress contribution due to the formation of phason defects.
- The athermal stress component due to the elastic interaction between dislocations, estimated from the dislocation density, is relatively small compared to the total flow stress, in particular at low temperatures. The elastic limit together with the athermal stress component explain the flow stress during steady state flow at high temperatures.
- At low temperatures, very strong work-hardening yields very high flow stresses, which cannot be explained by the stress components mentioned above. The nature of the respective additional flow stress component has to be determined in future experiments.

Acknowledgements

The authors wish to thank Prof. J. Kirschner for supporting these studies. They are grateful to Prof. K. Urban and Drs. M. Feuerbacher and P. Schall from Jülich Research Centre for supplying the single quasicrystal material and for the long-lasting cooperation. They also thank the Deutsche Forschungsgemeinschaft (DFG) for financial support.

References

[1] M. Bartsch, B. Geyer, D. Häussler, M. Feuerbacher, K. Urban, U. Messerschmidt, Mater. Sci. Eng. 294–296 (2000) 761.
[2] M. Wollgarten, M. Beyss, K. Urban, H. Liebertz, U. Köster, Phys. Rev. Lett. 71 (1993) 549.
[3] M. Feuerbacher, B. Baufeld, R. Rosenfeld, M. Bartsch, G. Hanke, M. Beyss, M. Wollgarten, U. Messerschmidt, K. Urban, Phil. Mag. Lett. 71 (1995) 91.
[4] B. Geyer, M. Bartsch, M. Feuerbacher, K. Urban, U. Messerschmidt, Phil. Mag. A 80 (2000) 1151.
[5] U. Messerschmidt, M. Bartsch, B. Geyer, M. Feuerbacher, K. Urban, Phil. Mag. A 80 (2000) 1165.
[6] D. Brunner, D. Plachke, H.D. Carstanjen, Mater. Sci. Eng. A 234–236 (1997) 310.
[7] D. Brunner, D. Plachke, H.D. Carstanjen, Mater. Sci. Eng. A 294 (2000) 773.
[8] M. Wollgarten, M. Bartsch, U. Messerschmidt, M. Feuerbacher, R. Rosenfeld, M. Beyss, K. Urban, Phil. Mag. Lett. 71 (1995) 99.
[9] D. Caillard, F. Mompiou, L. Bresson, D. Gratias, Scripta Mater. 49 (2003) 11.
[10] F. Mompiou, L. Bresson, P. Cordier, D. Caillard, Phil. Mag. 83 (2003) 3133.
[11] U. Messerschmidt, M. Bartsch, B. Geyer, L. Ledig, in: H.R. Trebin (Ed.), Quasicrystals, Wiley/VCH, Weinheim, 2003, p. 462.
[12] U. Messerschmidt, L. Ledig, M. Bartsch, J. Non-Cryst. Solids 334/335 (2004) 436.
[13] M. Feuerbacher, C. Metzmacher, M. Wollgarten, K. Urban, B. Baufeld, M. Bartsch, U. Messerschmidt, Mater. Sci. Eng. A 226 (1997) 943.
[14] M. Feuerbacher, C. Metzmacher, M. Wollgarten, K. Urban, B. Baufeld, M. Bartsch, U. Messerschmidt, Mater. Sci. Eng. A 233 (1997) 103.
[15] U. Messerschmidt, M. Bartsch, M. Feuerbacher, B. Geyer, K. Urban, Phil. Mag. A 79 (1999) 2123.
[16] S. Takeuchi, T. Hashimoto, Jpn. J. Appl. Phys. 32 (1993) 2063.
[17] U. Messerschmidt, D. Häussler, M. Bartsch, B. Geyer, M. Feuerbacher, K. Urban, Mater. Sci. Eng. A 294 (2000) 757.
[18] G.I. Taylor, Proc. R. Soc. 145 (1934) 362.
[19] U. Messerschmidt, B.V. Petukhov, M. Bartsch, Ch. Dietzsch, B. Geyer, D. Häussler, L. Ledig, M. Feuerbacher, P. Schall, K. Urban, Mater. Sci. Eng. A 319–321 (2001) 107.
[20] R.K. Ham, Phil. Mag. 6 (1961) 1183.
[21] R. Rosenfeld, Diploma Thesis, Aachen, 1994.
[22] P. Schall, M. Feuerbacher, M. Bartsch, U. Messerschmidt, K. Urban, Phil. Mag. Lett. 79 (1999) 785.
[23] U.F. Kocks, Physical basis for non-elastic constitutive relations, Discussion Paper at Symp. Adv. in Metal Deformation, Cornell Univ., Ithaca, 1976. J. Eng. Mater. Technol. 98 (1976) 76.
[24] K. Tanaka, Y. Mitarai, M. Koiwa, Phil. Mag. A 73 (1996) 1715.
[25] R. Rosenfeld, M. Feuerbacher, B. Baufeld, M. Bartsch, M. Wollgarten, G. Hanke, M. Beyss, U. Messerschmidt, K. Urban, Phil. Mag. Lett. 72 (1995) 375.

[26] F. Mompiou, D. Caillard, M. Feuerbacher, Phil. Mag. 84 (2004) 2777.
[27] M. de Boisseu, H. Takakura, A.P. Tsai, Poster at Eighth International Conference on Quasicrystals, Bangalore, 2002.
[28] J.P. Hirth, J. Lothe, Theory of Dislocations, Wiley, New York, 1982.
[29] P. Guyot, G. Canova, in: S. Takeuchi, T. Fujiwara (Eds.), Quasicrystals, World Scientific, Singapore, 1998, p. 529.
[30] M. Feuerbacher, P. Schall, Y. Estrin, Y. Bréchet, Phil. Mag. Lett. 81 (2001) 473.
[31] F. Mompiou, Doctoral Thesis, Toulouse, 2004.
[32] F. Baier, M.A. Müller, B. Grushko, H.-E. Schaefer, Mater. Sci. Eng. 294–296 (2000) 650.
[33] H. Mehrer, R. Galler, J. Alloys Compd. 342 (2002) 296.